Inorganic Chemistry
Article

Inorg. Chem. **2010**, *49*, 7969–7975 **7969**
DOI: 10.1021/ic100880j

Two 3D Triazolate−Tricarboxylate-Bridged $Cu^{II/I}$ Frameworks by One-Pot Hydrothermal Synthesis Exhibiting Spin-Canted Antiferromagnetism and Strong Antiferromagnetic Couplings

En-Cui Yang,* Zhong-Yi Liu, Xiang-Jun Shi, Qing-Qing Liang, and Xiao-Jun Zhao*

College of Chemistry, Tianjin Key Laboratory of Structure and Performance for Functional Molecule, Tianjin Normal University, Tianjin 300387, People's Republic of China

Received May 4, 2010

Two 3D coordination polymers with the same components but different structures, $[Cu^{II}_2Cu^{I}(trz)_3(Hbtc)]_n$ (**1**) and $[Cu_4(Htrz)_2(\mu_3\text{-}OH)_2(btc)_2]_n$ (**2**), were obtained together by a one-pot hydrothermal reaction of $Cu(OAc)_2 \cdot H_2O$, 1,2,4-triazole (Htrz), and 1,3,5-benzenetricarboxylic acid (H_3btc). Complex **1** is a mixed-valence $Cu^{I/II}$ honeycomb built from wavy Cu^{II}−trz−carboxylate layers and Cu^{I} nodes with doubly deprotonated $Hbtc^{2-}$ ligands covalently filled in the channels. In contrast, **2** is a tetranuclear $[Cu_4(Htrz)_2(\mu_3\text{-}OH)_2]^{6+}$ cluster-based framework extended by a fully deprotonated btc^{3-} ligand, displaying a 3,6-connected topological network. More interestingly, spin-canted antiferromagnetism and overall strong antiferromagnetic couplings up to $-147.1\ cm^{-1}$ are respectively observed for **1** and **2**, which are significantly due to the antisymmetric magnetic exchange in the wavy Cu^{II}−trz−carboxylate sublayer of **1** and the cooperative 4-fold heterobridges within the tetranuclear cluster of **2**.

Introduction

The construction of multidimensional hybrid organic−inorganic materials with interesting magnetic couplings has become one of the major challenges in inorganic and materials chemistry.[1,2] Because the organic ligands can behave as effective superexchange pathways to communicate various magnetic information between the spin carriers, commonly short bridges (azide,[3−5] oxalate,[6] cyanide,[7] dicyanamide,[8] tri-[9−13]/tetrazolate,[14−20] and formate[21]) have been extensively used for molecular magnets for their rich and varied coordination characteristics, bridging modes, as well as well-suited distance for efficiently transmitting magnetic couplings between two spins.[22] Very recently, because of the significant collaboration and/or competition among different

*To whom correspondence should be addressed. E-mail: xiaojun_zhao15@yahoo.com.cn (X.-J.Z.); encui_yang@yahoo.com.cn (E.-C.Y.).

(1) Kahn, O. *Molecular Magnetism*; VCH: Weinheim, Germany, 1993. (b) Kurmoo, M. *Chem. Soc. Rev.* **2009**, *38*, 1353.
(2) Coronado, E.; Forment-Aliaga, A.; Galan-Mascaros, J. R.; Giminez-Saiz, C.; Gomez-Garcia, C. J.; Martinez-Ferrero, E.; Nunez, A.; Romero, F. M. *Solid State Sci.* **2003**, *5*, 917.
(3) Zeng, Y.-F.; Hu, X.; Liu, F.-C.; Bu, X.-H. *Chem. Soc. Rev.* **2009**, *38*, 469.
(4) Yoon, J. H.; Ryu, D. W.; Kim, H. C.; Yoon, S. W.; Suh, B. J.; Hong, C. S. *Chem.—Eur. J.* **2009**, *15*, 3661.
(5) Triki, S.; Gómez-García, J. C.; Ruiz, E.; Sala-Pala, J. *Inorg. Chem.* **2005**, *44*, 5501.
(6) Gruselle, M.; Thouvenot, R.; Malézieux, B.; Train, C.; Gredin, P.; Demeschik, T. V.; Troitskaya, L. L.; Sokolov, V. I. *Chem.—Eur. J.* **2004**, *10*, 4763.
(7) (a) Ohba, M.; Ōkawa, H. *Coord. Chem. Rev.* **2000**, *198*, 313, and references therein. (b) Černák, J.; Orendáč, M.; Potočňák, I.; Chomič, J.; Orendáčová, A.; Skoršepa, J.; Feher, A. *Coord. Chem. Rev.* **2002**, *224*, 51.
(8) Miller, J. S.; Manson, L. L. *Acc. Chem. Res.* **2001**, *34*, 563.
(9) Quellette, W.; Galán-Mascarós, J. R.; Dunbar, K. R.; Zubieta, J. *Inorg. Chem.* **2006**, *45*, 1909.
(10) (a) Quellette, W.; Yu, M.-H.; O'Connor, C. J.; Hagrman, D.; Zubieta, J. *Angew. Chem., Int. Ed.* **2006**, *45*, 3497. (b) Quellette, W.; Prosvirin, A. V.; Chieffo, V.; Dunbar, K. R.; Hudson, B.; Zubieta, J. *Inorg. Chem.* **2006**, *45*, 9346.
(11) Verelst, M.; Sommier, L.; Lecante, P.; Mosset, A.; Kahn, O. *Chem. Mater.* **1998**, *10*, 980.
(12) Ding, B.; Yi, L.; Cheng, P.; Liao, D.-Z.; Yan, S.-P. *Inorg. Chem.* **2006**, *45*, 5799.
(13) Garcia, Y.; Van Koningsbruggen, P. J.; Bravic, G.; Guionneau, P.; Chasseau, D.; Cascarano, G. L.; Moscovici, J.; Lambert, K.; Michalowicz, A.; Kahn, O. *Inorg. Chem.* **1997**, *36*, 6357.
(14) Zhang, X.-M.; Jiang, T.; Wu, H.-S.; Zeng, M.-H. *Inorg. Chem.* **2009**, *48*, 4536.
(15) Zhou, J.-H.; Cheng, R.-M.; Song, Y.; Li, Y.-Z.; Yu, Z.; Chen, X.-T.; Xue, Z.-L.; You, X.-Z. *Inorg. Chem.* **2005**, *44*, 8011.
(16) (a) Haasnoot, J. G. *Coord. Chem. Rev.* **2000**, *200*, 131. (b) Klingele, M. H.; Brooker, S. *Coord. Chem. Rev.* **2003**, *241*, 119. (c) Beckmann, U.; Brooker, S. *Coord. Chem. Rev.* **2003**, *245*, 17.
(17) Bronisz, R. *Inorg. Chem.* **2007**, *46*, 6733.
(18) Song, W.-C.; Li, J.-R.; Song, P.-C.; Tao, Y.; Yu, Q.; Tong, M.-L.; Bu, X.-H. *Inorg. Chem.* **2009**, *48*, 3792.
(19) Lu, Y.-B.; Wang, M.-S.; Zhou, W.-W.; Xu, G.; Guo, G.-C. *Inorg. Chem.* **2008**, *47*, 8935.
(20) Yang, H.; Chen, J.-M.; Sun, J.-J.; Yang, S.-P.; Yu, J.; Tan, H.; Li, W. *Dalton Trans.* **2009**, *14*, 2540.
(21) Wang, Z.-M.; Zhang, B.; Fujiwara, H.; Kobayashi, H.; Kurmoo, M. *Chem. Commun.* **2004**, 416.
(22) Wang, X.-Y.; Wang, Z.-M.; Gao, S. *Chem. Commun.* **2008**, 281.
(23) Liu, T.; Zhang, Y.-J.; Wang, Z.-M.; Gao, S. *Inorg. Chem.* **2006**, *45*, 2782.
(24) Ma, Y.; Zhang, J.-Y.; Cheng, A.-L.; Sun, Q.; Gao, E.-Q.; Liu, C.-M. *Inorg. Chem.* **2009**, *48*, 6142.

Published on Web 07/28/2010

superexchange pathways, multiple heterobridged magnetic systems with mixed azide−carboxylate,[23−27] azide−tri/tetrazolate,[28,29] cyanide−dicyanamide,[30] and azide−cyanide mediatiors[8,31] have been successfully built by incorporating two or more structurally comparable ligands, which have exhibited various bulk magnetic behaviors (antiferromagnetism,[24,25] ferromagnetism,[24,32] spin canting,[28] metamagnetism,[23,31,32] and so on). However, successful magnetic examples with simultaneous 1,2,4-triazole (Htrz) and carboxylate, especially with trz- and benzene-based polycarboxylate bridges, have been scarcely observed by far[15,33] and would be hopefully expected because of the following two considerations. On the one hand, an individual trz or conjugated aromatic polycarboxylate ligand has been well-known as a component for the formation of multidimensional extended or discrete polynuclear complexes.[16,34,35] Magnetically, on the other hand, both the carboxylate and triazolyl groups have the capacity to favorably transmit different types of magnetic superexchange between the magnetic centers.[36] The trz ligand in metal complexes can adopt either a pyrazole-like μ_2-N1,N2-bridging fashion or an imidazole-like μ_2-N1,N4-bridging mode, and both can promote different antiferromagnetic couplings.[12,16,28] Moreover, the μ_2-N1,N2-bridging mode can make trz a superior linker in the construction of symmetric polynuclear subunits (binuclear, linear, and/or cyclic tri- and even tetranuclear structures).[15,16,37] In contrast, μ_2-N1,N4-trz could produce low-symmetry metal−trz−metal exchange pathways and thus potentially introduce the antisymmetric interaction for spin-canted antiferromagnetism.[28,36] The conformation-dependent carboxylate group can lead to different types of nature of magnetic couplings. Strongly antiferromagnetic with *syn*,*syn*-COO^-, very weakly and eventually ferromagnetic with *syn*,*anti*-COO^-, and weak-to-medium antiferromagnetic with *anti*,*anti*-COO^- have been widely observed.[32−40] Especially, long-range magnetic ordering can occur when paramagnetic metals were periodically extend into a 3D framework by multiple carboxylate bridges with different numbers and orientations.[32] Therefore, because of the possibly cooperative or competitive binding modes and magnetic superexchange pathways, combining trz- and benzene-based polycarboxylate bridges into one system could be an interesting approach to constructing promising materials with a high-dimensional-ordered skeleton and strong magnetic couplings. Herein, to continue the preparations of new molecular magnetic materials by a simple synthetic strategy, Htrz and 1,3,5-benzenetricarboxylic acid (H_3btc) were selected as mixed ligands to assemble with isotropic Cu^{II} ions under hydrothermal conditions. Two interesting 3D complexes with different appearances and comparably high thermal stability, a honeycomb-like mixed-valence $Cu^{I/II}$ framework for **1** and a tetranuclear cluster-based polymer for **2**, were obtained together. More importantly, **1** exhibits an interesting spin-canted antiferromagnetism arising from the antisymmetric magnetic exchange in a wavy Cu^{II}−trz−carboxylate sublayer. In contrast, complex **2** displays strong antiferromagnetic couplings up to -147.1 cm^{-1} resulting from multiple bridges with specific spatial orientations within the tetranuclear array.

Experimental Section

Materials and Instruments. All chemicals were commercially purchased (Htrz and H_3btc were from Acros, and other analytical-grade reagents were from Tianjin Chemical Reagent Factory) and used as received without further purification. Powder X-ray diffraction (PXRD) patterns were obtained from a Rigaku D/max-2500 diffractometer at 60 kV and 300 mA for Cu Kα radiation (λ = 1.5406 Å), with a scan speed of 2° min^{-1} and a step size of 0.02° in 2θ. The simulated PXRD patterns were calculated using single-crystal X-ray diffraction data and processed by the free *Mercury v1.4* program provided by the Cambridge Crystallographic Data Centre. Elemental analyses for carbon, hydrogen, and nitrogen were carried out with a CE-440 (Leeman-Laboratories) analyzer. Fourier transform (FT) IR spectra (KBr pellets) were taken on an Avatar-370 (Nicolet) spectrometer in the range 4000−400 cm^{-1}. Thermogravimetric analysis (TGA) experiments were performed on a Shimadzu simultaneous DTG-60A compositional analysis instrument from room temperature to 800 °C under a dinitrogen atmosphere at a heating rate of 5 °C min^{-1}. Magnetic susceptibilities were acquired on a Quantum Design (SQUID) magnetometer MPMS-XL-7 with crystalline samples, in which the phase purity of the samples were determined by PXRD experiments. The data were corrected for temperature-independent paramagnetism, and the diamagnetic corrections were calculated using Pascal's constants. An experimental correction for the sample holder was also applied.

Preparations of $C_{15}H_{10}Cu_3N_9O_6$ (1) and $C_{22}H_{14}Cu_4N_6O_{14}$ (2). $Cu(OAc)_2 \cdot H_2O$ (19.9 mg, 0.1 mmol), Htrz (13.9 mg, 0.2 mmol), and H_3btc (21.0 mg, 0.1 mmol) were dissolved in doubly deionized water (10 mL). The mixture was then transferred into

(25) (a) Zhao, J.-P.; Hu, B.-W; Yang, Q.; Zhang, X.-F.; Hu, T.-L.; Bu, X.-H. *Dalton Trans*. **2010**, *39*, 56. (b) Zhao, J.-P.; Hu, B.-W; Sañudo, E. C.; Yang, Q.; Zeng, Y.-F.; Bu, X.-H. *Inorg. Chem*. **2009**, *48*, 2482.
(26) Yu, Q.; Zeng, Y.-F.; Zhao, J.-P.; Yang, Q.; Hu, B.-W.; Chang, Z.; Bu, X.-H. *Inorg. Chem*. **2010**, *49*, 3746.
(27) Yu, Q.; Zeng, Y.-F.; Zhao, J.-P.; Yang, Q.; Hu, B.-W.; Chang, Z.; Bu, X.-H. *Inorg. Chem*. **2010**, *49*, 4301.
(28) Li, J.-R.; Yu, Q.; Sañudo, E. C.; Tao, Y.; Bu, X.-H. *Chem. Commun*. **2007**, 2602.
(29) Liu, P.-P.; Cheng, A.-L.; Liu, N.; Sun, W.-W.; Gao, E.-Q. *Chem. Mater*. **2007**, *19*, 2724.
(30) Zhang, Y.-Z.; Wang, Z.-M.; Gao, S. *Inorg. Chem*. **2006**, *45*, 10404.
(31) Zhang, Y.-Z.; Gao, S.; Sun, H.-L.; Su, G.; Wang, Z.-M.; Zhang, S.-W. *Chem. Commun*. **2004**, 1906.
(32) Lama, P.; Aijaz, A.; Sañudo, E. C.; Bharadwaj, P. K. *Cryst. Growth Des*. **2010**, *10*, 283.
(33) (a) Olea, D.; García-Couceiro, U.; Castillo, O.; Gómez-Herrero, J.; Zamora, F. *Inorg. Chim. Acta* **2007**, *360*, 48. (b) García-Couceiro, U.; Castillo, O.; Luque, A.; García-Terán, J. P.; Beobide, G.; Román, P. *Eur. J. Inorg. Chem*. **2005**, 4280.
(34) Eddaoudi, M.; Moler, D. B.; Li, H.-L.; Chen, B.-L.; Reineke, T. M.; O'keeffe, M.; Yaghi, O. M. *Acc. Chem. Res*. **2001**, *34*, 319.
(35) Zhang, J.-P.; Lin, Y.-Y.; Huang, X.-C.; Chen, X.-M. *J. Am. Chem. Soc*. **2005**, *127*, 5495.
(36) Rueff., J.-M.; Masciocchi, N.; Rabu, P.; Sironi, A.; Skoulios, A. *Chem.—Eur. J*. **2002**, *8*, 1813.
(37) (a) Zhai, Q.-G.; Lu, C.-Z.; Wu, X.-Y.; Batten, S. R. *Cryst. Growth Des*. **2007**, *7*, 2332. (b) Ouellette, W.; Prosvirin, A. V.; Valeich, J.; Dunbar, K. R.; Zubieta, J. *Inorg. Chem*. **2007**, *46*, 9067.
(38) (a) Karabach, Y. Y.; Kirillov, A. M.; Haukka, M.; Sanchiz, J.; Kopylovich, M. N.; Pombeiro, A. J. L. *Cryst. Growth Des*. **2008**, *8*, 4100. (b) Majumder, A.; Gramlich, V.; Rosair, G. M.; Batten, S. R.; Masuda, J. D.; El Fallah, M. S.; Ribas, J.; Sutter, J.-P.; Desplanches, C.; Mitra, S. *Cryst. Growth Des*. **2006**, *6*, 2355.
(39) (a) Humphrey, S. M.; Mole, R. A.; Thompson, R. I.; Wood, P. T. *Inorg. Chem*. **2010**, *49*, 3441. (b) Huang, Y.-G.; Yuan, D.-Q.; Pan, L.; Jiang, F.-L.; Wu, M.-Y.; Zhang, X.-D.; Wei, W.; Gao, Q.; Lee, J. Y.; Li, J.; Hong, M.-C. *Inorg. Chem*. **2007**, *46*, 9609. (c) Zheng, Y.-Z.; Xue, W.; Tong, M.-L.; Chen, X.-M.; Grandjean, F.; Long, G. J. *Inorg. Chem*. **2008**, *47*, 4077. (d) Caballo, R.; Covelo, B.; Salah El Fallah, M.; Ribas, J.; Vázquez-López, E. M. *Cryst. Growth Des*. **2007**, *7*, 1069. (e) Humphrey, S. M.; Alberola, A.; Gómez García, C. J.; Wood, P. T. *Chem. Commun*. **2006**, 1607. (f) Liu, T.-F.; Sun, H.-L.; Gao, S.; Zhang, S.-W.; Lau, T.-C. *Inorg. Chem*. **2003**, *42*, 4792.
(40) Arora, H.; Lloret, F.; Mukherjee, R. *Eur. J. Inorg. Chem*. **2009**, *22*, 3317.

Table 1. Crystal and Structure Refinement Data for **1** and **2**

	1	**2**
chemical formula	$C_{15}H_{10}Cu_3N_9O_6$	$C_{22}H_{14}Cu_4N_6O_{14}$
fw	602.94	840.55
cryst size (mm)	0.22 × 0.06 × 0.02	0.24 × 0.23 × 0.20
cryst syst	orthorhombic	monoclinic
space group	*Pbca*	$P2_1/n$
a (Å)	8.4471(6)	13.4823(15)
b (Å)	20.1912(14)	7.2714(8)
c (Å)	21.6010(14)	13.6596(15)
β (deg)	90	110.8500(10)
V (Å^3)	3684.2(4)	1251.4(2)
Z, D_c (g cm^{-3})	8, 2.174	2, 2.231
F(000)	2384	832
μ (mm^{-1})	3.494	3.445
data/restraints/params	3215/0/299	2209/0/208
GOF on F^2	1.049	1.029
R(int)	0.0449	0.0138
R1,[a] wR2[b] [$I > 2\sigma(I)$]	0.0265, 0.0602	0.0199, 0.0543
R1, wR2 (all data)	0.0350, 0.0640	0.0225, 0.0558
ρ_{max}, ρ_{min} (e Å^{-3})	0.897, − 0.592	0.562, − 0.360

[a] $R1 = \sum||F_o| - |F_c||/|F_o|$. [b] $wR2 = [\sum w(F_o^2 - F_c^2)^2/\sum w(F_o^2)^2]^{1/2}$.

a Parr Teflon-lined stainless steel vessel (23 mL) and heated at 160 °C for 72 h under autogenous pressure. After the mixture was cooled to room temperature at a rate of 5.6 °C h^{-1}, brown and blue block-shaped crystals for **1** (yield: 2.0 mg, 10% based on a Cu^{II} salt) and **2** (yield: 8.4 mg, 40% based on a Cu^{II} salt) were generated together and separated manually. Anal. Calcd for $C_{15}H_{10}Cu_3N_9O_6$ (**1**): C, 29.88; H, 1.67; N, 20.91. Found: C, 29.94; H, 1.63; N, 21.09. IR (KBr pellets, cm^{-1}): 3431(br), 3147(w), 1693(s), 1615(s), 1562(vs), 1543(s), 1501(s), 1452(s), 1429(s), 1375(s), 1294(s), 1272(m), 1253(s), 1231(s), 1192(s), 1156(s), 1067(m), 995(m), 758(m), 732(ms), 682(s), 670(s), 658(s), 546(w), 458(w). Anal. Calcd for $C_{22}H_{14}Cu_4N_6O_{14}$ (**2**): C, 31.44; H, 1.68; N, 10.00. Found: C, 31.42; H, 1.70; N, 10.01. IR (KBr, cm^{-1}): 3429(s), 3140(s), 2969(m), 2886(m), 2811(m), 1610(s), 1560(s), 1435(s), 1368(s), 1313(w), 1212(w), 1071(m), 894(w), 855(m), 775(m), 715(m), 629(m), 541(m), 488(w), 452(w).

Single-Crystal Structure Determination. Diffraction intensities for **1** and **2** were collected on a Bruker APEX-II CCD diffractometer equipped with graphite-monochromated Mo Kα radiation with a radiation wavelength of 0.710 73 Å by using the $\varphi-\omega$ scan technique at 296 K. There was no evidence of crystal decay during data collection. Semiempirical multiscan absorption corrections were applied by *SADABS*, and the program *SAINT* was used for integration of the diffraction profiles.[41] The structures were solved by direct methods and refined with the full-matrix least-squares technique using the *SHELXS-97* and *SHELXL-97* programs.[42] Non-H atoms were located by difference Fourier maps and subjected to anisotropic refinement. H atoms were added according to theoretical models. The crystallographic data and the selected bond lengths and angles are given in Tables 1−3, respectively.

TGA and PXRD of 1 and 2. Complexes **1** and **2** exhibit analogous compositional stability and are thermally stable up to ca. 328 °C (Figure S1 in the Supporting Information). The mixed ligands of the two complexes were continuously decomposed between 328 and 500 °C, leaving a 1:1 mixture of CuO−Cu_2O and a pure CuO powder as the final products for **1** and **2**, respectively (expt 36.8% and calcd 36.1% for **1**; expt 39.0% and calcd 37.8% for **2**). The phase purity of bulk products of the two complexes was further confirmed by PXRD (Figures S2 and S3 in the Supporting Information), which proved that the sample was the polycrystalline form of the desired complex.

Table 2. Selected Bond Lengths (Å) and Angles (deg) for **1**[a]

Cu1−N3	1.965(2)	Cu1−O1	1.966(2)
Cu1−N5$^{\#1}$	1.968(3)	Cu1−O5$^{\#2}$	1.977(2)
Cu2−N1	1.997(3)	Cu2−N7	2.002(3)
Cu2−N9$^{\#3}$	2.004(3)	Cu2−O6$^{\#4}$	2.035(2)
Cu2−N4	2.303(3)	Cu3−N6$^{\#5}$	1.916(3)
Cu3−N2	1.927(3)	Cu3−N8	2.119(3)
N3−Cu1−O1	91.70(10)	N3−Cu1−N5$^{\#1}$	179.35(11)
O1−Cu1−N5$^{\#1}$	88.09(10)	N3−Cu1−O5$^{\#2}$	88.88(10)
O1−Cu1−O5$^{\#2}$	177.67(9)	N5$^{\#1}$−Cu1−O5$^{\#2}$	91.35(10)
N1−Cu2−N7	93.16(11)	N1−Cu2−N9$^{\#3}$	171.25(11)
N7−Cu2−N9$^{\#3}$	91.87(11)	N1−Cu2−O6$^{\#4}$	85.44(10)
N7−Cu2−O6$^{\#4}$	166.03(10)	N9$^{\#3}$−Cu2−O6$^{\#4}$	87.95(10)
N1−Cu2−N4	92.64(10)	N7−Cu2−N4	99.53(11)
N9$^{\#3}$−Cu2−N4	93.58(10)	O6$^{\#4}$−Cu2−N4	94.42(9)
N6$^{\#4}$−Cu3−N2	147.25(12)	N6$^{\#5}$−Cu3−N8	115.49(12)
N2−Cu3−N8	97.17(11)		

[a] Symmetry codes: #1, $x - {}^1/_2, y, {}^3/_2 - z$; #2, ${}^3/_2 - x, y + {}^1/_2, z$; #3, $x + {}^1/_2, {}^1/_2 - y, 2 - z$; #4, $2 - x, y + {}^1/_2, {}^3/_2 - z$; #5, $2 - x, -y, 2 - z$.

Table 3. Selected Bond Lengths (Å) and Angles (deg) for **2**[a]

Cu1−O7$^{\#1}$	1.9236(16)	Cu1−O4$^{\#2}$	1.9545(17)
Cu1−O6$^{\#3}$	1.9823(16)	Cu1−N2	2.005(2)
Cu1−O7	2.2882(16)	Cu2−O6$^{\#5}$	2.2958(17)
Cu2−O3$^{\#4}$	1.9564(17)	Cu2−N1	1.987(2)
Cu2−O7$^{\#1}$	1.9261(16)	Cu2−O1	1.9272(18)
O4$^{\#2}$−Cu1−O6$^{\#3}$	94.66(7)	O7$^{\#1}$−Cu1−N2	87.76(7)
O4$^{\#2}$−Cu1−N2	88.89(8)	O6$^{\#3}$−Cu1−N2	166.67(8)
O7$^{\#1}$−Cu1−O7	84.11(6)	O4$^{\#2}$−Cu1−O7	95.30(7)
O6$^{\#3}$−Cu1−O7	78.44(6)	N2−Cu1−O7	114.08(7)
O7$^{\#1}$−Cu2−O1	173.55(8)	O7$^{\#1}$−Cu2−O3$^{\#4}$	91.10(7)
O1−Cu2−O3$^{\#4}$	90.83(8)	O7$^{\#1}$−Cu2−N1	88.01(7)
O1−Cu2−N1	89.16(8)	O3$^{\#4}$−Cu2−N1	171.44(8)
O7$^{\#1}$−Cu2−O6$^{\#5}$	79.36(6)	O1−Cu2−O6$^{\#5}$	106.46(8)
O3$^{\#4}$−Cu2−O6$^{\#5}$	98.00(7)	N1−Cu2−O6$^{\#5}$	90.20(7)
O7$^{\#1}$−Cu1−O6$^{\#3}$	89.08(7)		

[a] Symmetry codes: #1, $2 - x, 2 - y, 1 - z$; #2, $x + 1, y, z$; #3, $x + {}^1/_2, {}^5/_2 - y, z - {}^1/_2$; #4, $1 - x, 2 - y, 1 - z$; #5, ${}^3/_2 - x, y - {}^1/_2, {}^3/_2 - z$.

Results and Discussion

Syntheses and IR Spectra. The hydrothermal reaction of Htrz, H_3btc, and an inorganic Cu^{II} salt in a molar ratio of 2:1:1 at 160 °C for 72 h afforded simultaneously brown and blue block-shaped crystals **1**, $[Cu^{II}_2Cu^{I}(trz)_3(Hbtc)]_n$, and **2**, $[Cu_4(Htrz)_2(\mu_3\text{-}OH)_2(btc)_2]_n$. Obviously, part of the raw divalent Cu^{II} source was reduced to a monovalent Cu^{I} ion under hydrothermal conditions.[43] In contrast to **2**, the strong IR absorption located at 1693 cm^{-1} confirms the presence of an undeprotonated carboxylic group in **1**.

Crystal Structures of 1 and 2. X-ray single-crystal structural analysis suggests that **1** is a honeycomb-like 3D mixed-valence $Cu^{I/II}$−trz coordination polymer with the $Hbtc^{2-}$ ligand covalently filled in the channels. There are three crystallographically independent metal centers

(41) *SAINT Software Reference Manual*; Bruker AXS: Madison, WI, 1998.
(42) (a) Sheldrick, G. M. *SHELXL-97, Program for X-ray Crystal Structure Refinement*; Göttingen University: Göttingen, Germany, 1997. (b) Sheldrick, G. M. *SHELXS-97, Program for X-ray Crystal Structure Solution*; Göttingen University: Göttingen, Germany, 1997.

(43) (a) Wang, W.-J.; Xu, L.; Gao, G.-G..; Liu, X.-Z.; Liu, L. *Inorg. Chem. Commun.* **2009**, *12*, 259. (b) Guo, H.-X.; Li, X.-Z.; Huang, S.-K.; Ling, Y.; Weng, W. *Inorg. Chem. Commun.* **2010**, *13*, 262. (c) Tao, J.; Zhang, Y.; Tong, M.-L.; Chen, X.-M.; Yuen, T.; Lin, C.-L.; Huang, X.-Y.; Li, J. *Chem. Commun.* **2002**, 1342. (d) Zhang, X.-M.; Tong, M.-L.; Chen, X.-M. *Angew. Chem., Int. Ed.* **2002**, *41*, 1029. (e) Colacio, E.; Kivekäs, R.; Lloret, F.; Sunberg, M.; Suarez-Varela, J.; Bardaji, M.; Laguna, A. *Inorg. Chem.* **2002**, *41*, 5141. (f) Tong, M.-L.; Li, L.-J.; Mochizuki, K.; Chang, H.-C.; Chen, X.-M.; Li, Y.; Kitagawa, S. *Chem. Commun.* **2003**, 428. (g) Kang, Y.; Yao, Y.-G.; Qin, Y.-Y.; Zhang, J.; Chen, Y.-B.; Li, Z.-J.; Wen, Y.-H.; Cheng, J.-K.; Hu, R. F. *Chem. Commun.* **2004**, 1046.

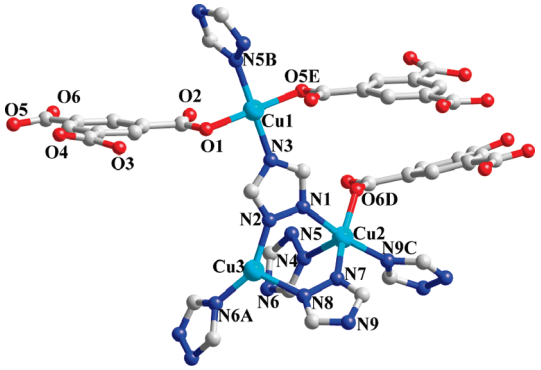

Figure 1. Local coordination environments of $Cu^{II/I}$ atoms in **1**. The H atoms were omitted for clarity. Symmetry codes: A = $2-x, -y, 2-z$; B = $x-0.5, y, 1.5-z$; C = $0.5+x, 0.5-y, 2-z$; D = $2-x, 0.5+y, 1.5-z$; E = $2-x, -y, 2-z$.

(two Cu^{II} ions and one Cu^{I} ion), three deprotonated trz anions, and one doubly deprotonated $Hbtc^{2-}$ ligand in the asymmetric unit of **1**. As shown in Figure 1, the divalent Cu1 site is surrounded by two individual monodentate carboxylate O (O1 and O5E) and two separate trz N (N3 and N5B) donors to finish the square-planar coordination geometry. The divalent Cu2 atom is in a distorted square-pyramidal geometry, coordinating to one carboxylate O atom from one $Hbtc^{2-}$ anion and four different trz N donors (N4, N1, N7, and N9C). While a monovalent Cu3 ion is in a distorted planar triangle (see Table 2) defined by three separate trz N atoms (N2, N8, and N6A). All of the bond lengths and angles around the metal ions are comparable with the previous values (see Table 2).[44]

In the crystal lattice of **1**, three tridentate trz groups and one carboxylate group of $Hbtc^{2}$ ligands connect the divalent Cu^{II} ions into a wavy $Cu^{II}-trz-COO^{-}$ sublayer in the crystallographic *ac* plane (Figure 2a,b), which are further fused face-to-face by monovalent Cu^{I} ions. As a result, a 3D honeycomb framework was generated with $Hbtc^{2-}$ anions covalently filled in the channels by Cu−O coordination bonds (Figure 2c). Notably, the divalent Cu1 and Cu2 ions within the $Cu^{II}-trz-COO^{-}$ sublayer are alternately connected into a 1D chain by single trz connectors and doubly trz and *syn,anti*-COO^{-} bridges (Figure 2b), which are further linked by the third crystallographic unique trz ligands into a magnetically active sublayer of **1** with intermetallic separations of 3.5992(1), 5.99873, and 6.0090(3) Å for Cu1····Cu2A, Cu1····Cu2, and Cu2····Cu2G, respectively. Obviously, four three-atom bridges (three trz and one *syn,anti*-COO^{-}) become the significant magnetic superexchange pathways between Cu1 and Cu2 (Figure S4 in the Supporting Information).

Complex **2** crystallizes in the monoclinic space group $P2_1/n$, displaying a tetranuclear cluster-based 3D network extended by fully deprotonated btc^{3-} linkers. As shown in Figure 3a, the secondary building unit (SBU) of **2** contains a cationic $[Cu_4(Htrz)_2(\mu_3\text{-}OH)_2]^{6+}$ cluster with a center of inversion and two symmetry-related btc^{3-} connectors. The tetranuclear cluster consists of two pairs of square-pyramidal Cu^{II} ions (Cu1 and Cu2), a couple of neutral μ_2-N1,N2-bridging Htrz ligands, and two tridentate hydroxyl groups. The basal plane of the square-pyramid Cu1 atom is well-defined by two carboxylate O atoms from two individual btc^{3-} ligands, one μ_3-OH group, and one N donor from the μ_2-N1,N2-Htrz ligand, while the axial site is occupied by another μ_3-OH (see Figure S5 in the Supporting Information). By contrast, the basal sites of the Cu2 ion are occupied by one μ_3-OH group, two separate carboxylate O donors from two different btc^{3-} anions, and one N atom from a neutral μ_2-N1,N2-Htrz molecule. The apical position is occupied by a carboxylate O atom from the btc^{3-} ligand. The Cu−O bond lengths in the apical positions are considerably longer (0.3 Å) than the Cu−O and/or Cu−N separations in the basal plane (see Table 3).

A pair of symmetry-related μ_3-OH groups doubly hold three separate Cu^{II} ions together, generating a centrosymmetric tetranuclear $[Cu_4(Htrz)_2(\mu_3\text{-}OH)_2]^{6+}$ cluster with a pair of μ_2-N1,N2-bridging Htrz ligands consolidating the Cu1 and Cu2 ions in the asymmetric unit. The Cu^{II} ions in the tetranuclear cluster is in a parallelogram-shaped arrangement, which is analogous to those previously reported tetrazole-1-acetic acid based Cu^{II} complexes.[45] The intermetallic separations within the cluster are 3.3598(5), 3.1369(4), and 3.0975(5) Å for Cu1···Cu2, Cu1···Cu1A, and Cu1···Cu2A, respectively.

Acting as a 3-connected node, the sole crystallographic independent btc^{3-} ligand in **2** presents its three carboxylate groups to aggregate three neighboring clusters by *syn,anti*-bidentate and *syn,syn*-monodentate bridging and terminally monodentate coordination modes (Figures 3b and S6 in the Supporting Information). On the other hand, each of the tetranuclear clusters is surrounded by six btc^{3-} ligands and can be considered as a 6-connected topological node (Figures 3b and S6 in the Supporting Information). Finally, the overall structure of **2** is a 3,6-connected *rtl* network with the Schläfli symbol of $(4.6^2)_2(4^2.6^{10}.8^3)$. It should be noted that the nearest $Cu^{II}\cdots Cu^{II}$ distance spanned by the btc^{3-} ligand is 6.6914(6) Å in the overall 3D network of **2**, which is obviously far from those within the tetranuclear cluster. Therefore, the significant magnetic couplings transmitted by the mixed 4-fold μ_3-OH, μ_2-N1,N2-Htrz, and *syn,anti*- and *syn,syn*-COO^{-} bridges can hopefully be expected within the tetranuclear cluster of **2** (Figure 3c).

Magnetic Properties. The variable-temperature magnetic susceptibilities of **1** and **2** were measured on crystalline samples in an applied direct-current (dc) magnetic field of 2000 Oe in the range 2−300 K. As shown in Figure 4, the $\chi_M T$ value of **1** at 300 K is 0.74 cm^3 K mol^{-1}, indicating strong antiferromagnetic interactions even at room temperature. $\chi_M T$ decreases continuously with a lowering of the temperature and reaches a minimum of 0.07 cm^3 K mol^{-1} at 10 K. Upon further cooling to 2 K, $\chi_M T$ rises abruptly to a sharp maximum of 0.18 cm^3 K mol^{-1} at 7 K and finally drops rapidly. This behavior suggests a spin-canted antiferromagnetism at low temperature. The abrupt increase at 7 K indicates the onset of magnetic

(44) (a) Zhang, X.-M.; Fang, R.-Q. *Inorg. Chem.* **2005**, *44*, 3955. (b) Deng, H.; Qiu, Y.-C.; Daiguebonne, C.; Kerbellec, N.; Guillou, O.; Zeller, M.; Batten, S. R. *Inorg. Chem.* **2008**, *47*, 5866. (c) Chou, C.-C.; Su, C.-C.; Yeh, A. *Inorg. Chem.* **2005**, *44*, 6122. (d) Kim, D.-H.; Koo, J.-E.; Hong, C. S.; Oh, S.; Do, Y. *Inorg. Chem.* **2005**, *44*, 4383. (e) Yang, H.-X.; Guo, S.-P.; Tao, J.; Lin, J.-X.; Cao, R. *Cryst. Growth Des.* **2009**, *9*, 4735. (f) Okubo, T.; Tanaka, N.; Kim, K. H.; Yone, H.; Maekawa, M.; Kuroda-Sowa, T. *Inorg. Chem.* **2010**, *49*, 3700.

(45) Yu, Q.; Zhang, X.-Q.; Bian, H.-D.; Liang, H.; Zhao, B.; Yan, S.-P.; Liao, D.-Z. *Cryst. Growth Des.* **2008**, *8*, 1140.

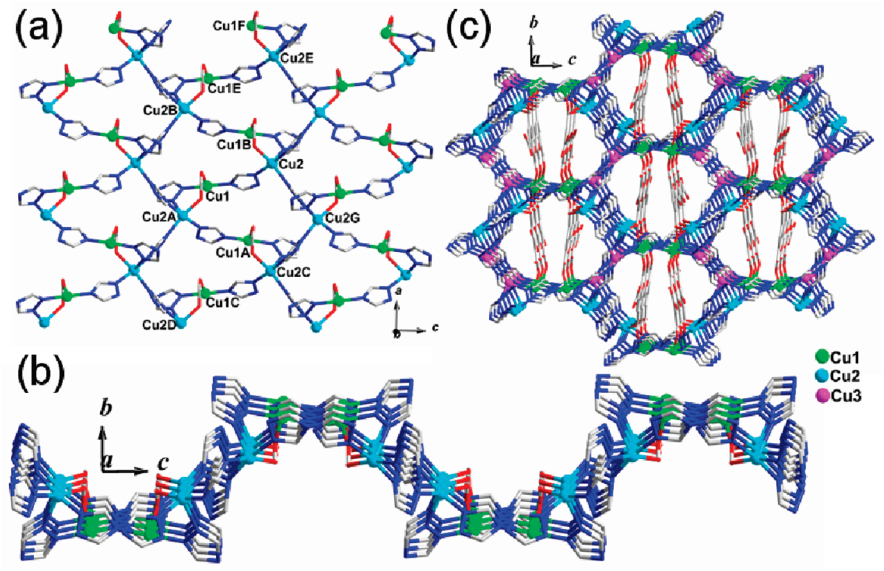

Figure 2. (a) 2D Cu^{II}−trz−COO^- sublayer of **1** viewed along the *b* axis. Symmetry codes: A = $x - 0.5, y, 1.5 - z$; B = $0.5 + x, y, 1.5 - z$; C = $x - 1, y, z$; D = $x - 1.5, y, 1.5 - z$; E = $1 + x, y, z$; F = $1.5 + x, y, 1.5 - z$; G = $x - 0.5, 0.5 - y, 2 - z$. (b) 2D Cu^{II}−trz−COO^- sublayer of **1** viewed along the *a* axis. (c) 3D honeycomb framework of **1**.

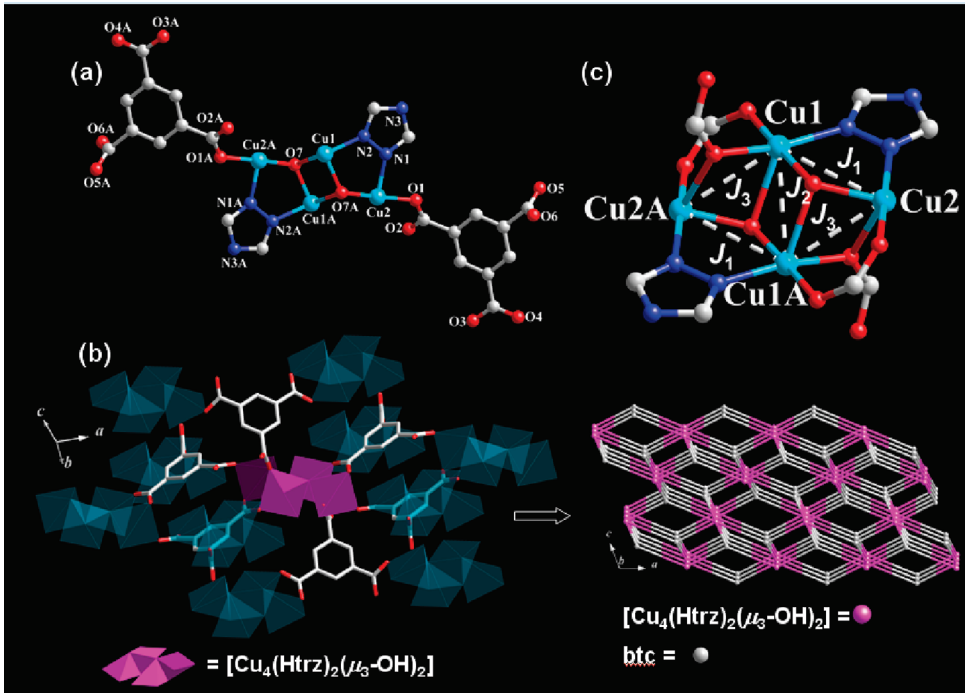

Figure 3. (a) Tetranuclear SBU of **2**. The H atoms were omitted for clarity. Symmetry code: A = $2 - x, 2 - y, 1 - z$. (b) View of the linkages of a tetranuclear Cu^{II} cluster (purple) with 10 neighboring clusters (blue) by six btc^{3-} ligands and the 3,6-connected 3D topological structure of **2**. (c) Magnetic tetranuclear cluster of **2**.

order with a spontaneous magnetization, and the second drop of $\chi_M T$ below 7 K may arise from interlayer antiferromagnetic interactions. Above 100 K, the plot of χ_M^{-1} vs T obeys the Curie−Weiss law with $C = 0.824\ cm^3\ K\ mol^{-1}$ and $\theta = -40.85$ K, indicating the presence of antiferromagnetic coupling between the Cu^{II} ions. Obviously, the superexchange pathways of **1** originate structurally from the Cu^{II}−trz−carboxylate layer. When the superexchange pathways through the Cu^{I} ions are discounted, the magnetic data of **1** were fitted by a Heisenberg alternating chain model ($\mathbf{H} = -2J\sum_1[S_{2i}S_{2i-1} + \alpha S_{2i}S_{2i+1}]$) for $S = {}^1/_2$ between 14 and 300 K, in which the molecule-field approximation was introduced to evaluate the interchain interactions (zJ') (see Table S1 in the Supporting Information).[1,46] Also, the results of the best fit were $g = 2.12$, $J = -32.84\ cm^{-1}$, $\alpha = 0.685$, $zJ' = -16.95\ cm^{-1}$, and $R = 4.1 \times 10^{-4}$. Undoubtedly, the higher J than αJ and zJ' confirms that the antiferromagnetic couplings in **1** can be dominantly attributed to the double *syn*,*anti*-COO^- and μ_2-N1,N2-trz bridges. On the other hand, the round maximum at 28 K in the $\chi_M - T$ plot

(46) Olmstead, M. M.; Musker, W. K.; Ter Haar, L. W.; Hatfield, W. E. *J. Am. Chem. Soc.* **1982**, *104*, 6627.

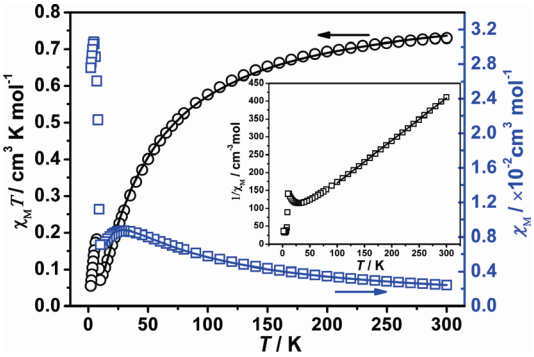

Figure 4. Temperature dependence of $\chi_M T$, χ_M, and χ_M^{-1} (inset) for **1**. The solid lines represent the best fit to a two-site model with alternating exchange.

suggests the presence of short-range antiferromagnetic ordering within the 2D Cu^{II}−trz−carboxylate sublayer. Both of the $\chi_M T$ and χ_M vs T plots below 9 K are strongly field-dependent (Figure S7 in the Supporting Information), consistent with spin canting.

Evidence for the magnetic phase transition was confirmed by field-cooled (FC)/zero-field-cooled (ZFC) measurements (H_{dc} = 100 Oe) and alternating-current (ac) susceptibility. Results of the FC and ZFC measurements (Figure 5a) at 100 Oe exhibit a maximum at 5.6 K (T_N). Above T_N, the magnetization is reversible and behaves similarly for both FC and ZFC. Below T_N, however, there is nonreversibility and bifurcation, consistent with spontaneous magnetization below a phase transition. The divergence of FC and ZFC indicates a history dependence of the magnetization process. The ZFC ac susceptibility measurements performed in the range of 100 Hz to 1 kHz at H_{ac} = 3.5 Oe below 15 K (Figure 5b) show that both the χ' and χ'' signals have sharp maxima at 5.7 K. No frequency dependence was observed, which excludes the possibility of the spin glass in **1**.[47]

The field dependence of magnetization, $M(H)$, at 2 K (Figure S8 in the Supporting Information) is consistent with a spin-canted antiferromagnetic behavior, and there is an abrupt increase of magnetization with the fields below 1.6 kOe, and then magnetization steadily increases linearly with the field up to 0.0744 Nβ at 50 kOe but without reaching saturation (2 Nβ for two Cu^{II} ions). At 2 K, **1** exhibits a magnetic hysteresis loop with a coercive field of 100 Oe and a remnant magnetization of 0.0011 Nβ. The spontaneous magnetization observed is due to the spin canting with an estimated canting angle of 0.03° [$\psi = \tan^{-1}(M_r/M_s)$].[28,48] Structurally, spin canting is usually caused by either single-ion magnetic anisotropy or antisymmetric magnetic exchange in magnetic entities.[28] For **1**, the observed spin canting may be attributed to the antisymmetric magnetic exchange within the 2D Cu^{II}−trz−COO^-, which are scarcely reported for the extended Cu^{II} complexes.[49−52] Although the structure has an inversion center located at the Cu^I position of the interlayer, the crystallographic symmetric operations (2-fold screw axis and glide plane) within the 2D Cu^{II}−trz−COO^- sublayer induce antisymmetric magnetic exchanges, which are responsible for the spin canting of **1**.

2 exhibited temperature-dependent behavior quite different from that of **1** (Figure 6). The $\chi_M T$ value for each tetranuclear cluster is 1.07 cm^3 K mol^{-1} at 300 K, which is far below the spin-only value of 1.5 cm^3 K mol^{-1} expected for four noninteracting Cu^{II} ions with g = 2.0. As the temperature decreases, $\chi_M T$ decreases slowly to a minimum value (0.020 cm^3 K mol^{-1}) at 2 K. This behavior is characteristic of a strong antiferromagnetic exchange interaction between the paramagnetic metal ions. Notably, the sharp increase of χ_M below 75 K suggests the existence of a small mount of paramagnetic impurity.

Because of the presence of a couple of unsymmetrical μ_3-OH bridges within the tetranuclear unit, three exchange integrals, J_1, J_2, and J_3, are required to describe each possible pairwise exchange interaction between two adjacent Cu^{II} ions. S_1, S_2, S_{1A}, and S_{2A} correspond to the spin operators of Cu1, Cu2, Cu1A, and Cu2A, respectively. Hence, on the basis of a superexchange mode represented in Figure 3c, the spin Hamiltonian equation

$$\mathbf{H} = -2J_1(S_1S_2 + S_{1A}S_{2A}) - 2J_2S_1S_{1A} - 2J_3(S_1S_{2A} + S_{1A}S_2) \quad (1)$$

is used to fit the experimental magnetic data of **2**. The resulting energy matrix can be solved[53] and an expression for the molar magnetic susceptibility derived from the van Vleck equation (see Table S2 in the Supporting Information). The best-fit parameters are g = 2.12, J_1 = −147.1 cm^{-1}, J_2 = 9.5 cm^{-1}, J_3 = −24 cm^{-1}, and ρ (the percentage of paramagnetic impurity) = 2.31%, with R = 6.2 × 10^{-4}, where R is the agreement factor defined as $\sum[(\chi_M T)_{obsd} - (\chi_M T)_{calcd}]^2/\sum[(\chi_M T)_{obsd}]^2$.

To assign quantitatively the superexchange coupling to different bridges, the magnetostructural correlation should be analyzed. The unpaired electron of each square-pyramidal Cu^{II} center is in a d(x^2-y^2)-type magnetic orbital, which is located in the basal plane of the square pyramid. However, the unpaired electron density along the d(z^2) orbital is quite low; the magnetic exchange through the apical pathway is thus expected to very little. Meanwhile, it is well-known that the magnetic interaction in the double μ_3-OH-bridged Cu^{II} systems is sensitive to the Cu−O−Cu angle.[54,55] In **2**, the strongest antiferromagnetic coupling for J_1 should be ascribed to the superexchange pathways by double μ_3-OH and $\mu_{1,2}$-Htrz bridges because they both locate at the basal positions of the Cu1 or Cu2 ions. In contrast, the poor overlap between the orbitals of the Cu^{II} centers and the two apical μ_3-OH bridges, together with the specific bond angle (95.89°) of Cu1−O7−Cu1A, is

(47) Mydosh, J. A. *Spin Glasses: An Experimental Introduction*; Taylor and Francis: London, 1993.
(48) Palacio, F.; Andres, M.; Horne, R.; Van Duynevelt, A. J. *J. Magn. Magn. Mater.* **1986**, *54*, 1487.
(49) Navarro, J. A. R.; Barea, E.; Rodríguez-Diéguez, A.; Salas, J. M.; Ania, C. O.; Parra, J. B.; Masciocchi, N.; Galli, S.; Sironi, A. *J. Am. Chem. Soc.* **2008**, *130*, 3978.
(50) Hu, K.-L.; Kurmoo, M.; Wang, Z.-M.; Gao, S. *Chem.—Eur. J.* **2009**, *15*, 12050.
(51) Dender, D. C.; Davidovic., D.; Reich, D. H.; Broholm, C.; Lefmann, K.; Aeppli, G. *Phys. Rev. B* **1996**, *53*, 2583.
(52) Park, S. H.; Lee, C. E. *Bull. Korean Chem. Soc.* **2006**, *27*, 1587.
(53) Song, Y.-F.; Massera, C.; Roubeau, O.; Gamez, P.; Lanfredi, A. M. M.; Reedijk, J. *Inorg. Chem.* **2004**, *43*, 6842.
(54) Buvaylo, E. A.; Kokozay, V. N.; Vassilyeva, O. Y.; Skelton, B. W.; Jezierska, J.; Brunel, L. C.; Ozarowski, A. *Inorg. Chem.* **2005**, *44*, 206.
(55) Zhu, X.; Zhao, J.-W.; Li, B.-L.; Song, Y.; Zhang, Y.-M.; Zhang, Y. *Inorg. Chem.* **2010**, *49*, 1266.

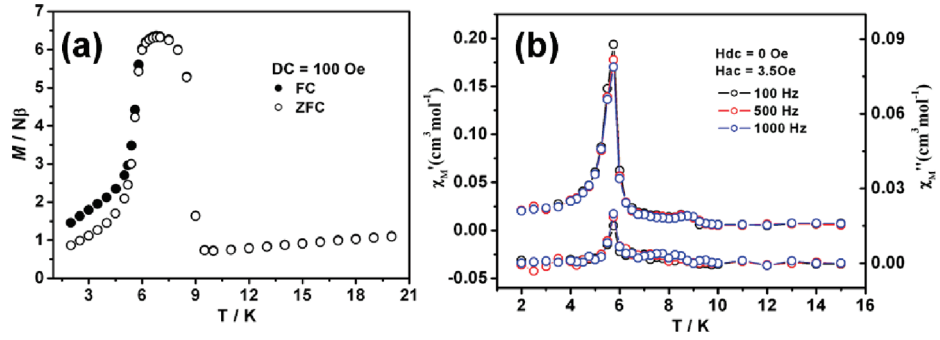

Figure 5. (a) FC and ZFC magnetization for **1**. (b) Real (χ') and imaginary (χ'') ac magnetic susceptibilities in a zero applied dc field and in an ac field of 3.5 Oe at different frequencies (100, 500, and 1000 Hz) for **1**.

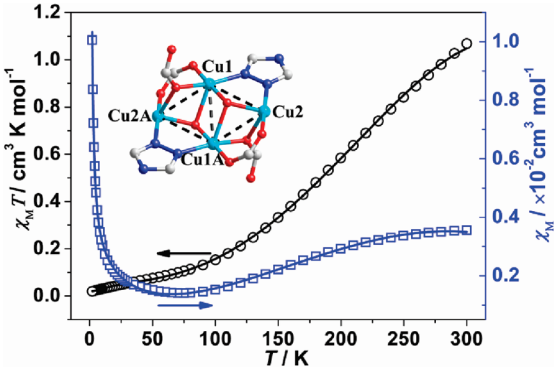

Figure 6. Temperature dependence of $\chi_M T$ and χ_M for **2**. Inset: definition of the magnetic exchange pathways for **2**. The solid lines represent the best fit to a tetranuclear model.

expected to transfer a small ferromagnetic coupling constant corresponding to J_2.[56] The moderate antiferromagnetic J_3 is associated with the triple bridges (*syn*,*anti*-COO^-, *syn*,*syn*-COO^-, and μ_3-OH). On the basis of the bonds angles of Cu1−O7−Cu2A and Cu1−O6−Cu2A (94.22° and 92.49°), the superexchange pathways by μ_3-OH and *syn*,*anti*-COO^- bridges transfer weak ferromagnetic coupling, which is overcompensated for by the strong antiferromagnetic coupling mediated by the *syn*,*syn*-COO^- bridge and contributes essentially to a negative coupling constant.[32,38−40] Obviously, different magnetic structures, the asymmetric magnetic exchange within the 2D Cu^{II}−trz−COO^- sublayer of **1**, and the symmetric tetranuclear Cu^{II} clusters built by μ_3-OH, μ_2-N1,N2-Htrz, *syn*,*anti*-COO^-, and *syn*,*syn*-COO^- bridges for **2** should be significantly responsible for their entirely different magnetic properties.

In summary, one-pot hydrothermal synthesis generates two different 3D molecular materials with distinct magnetic couplings. The 3D mixed-valence $Cu^{I/II}$ honeycomb of **1** displays spin-canted antiferromagnetism, while the 3D tetranuclear cluster-based, 3,6-connected framework of **2** behaves as strong antiferromagnetic couplings. These studies show that mixed benzene-based polycarboxylate−trz bridges are particularly remarkable for the design of high-dimensional networks with interesting bulk magnetic behaviors. Research on other paramagnetic metal complexes with mixed heterobridges and their magnetic studies are underway in our laboratory.

Acknowledgment. We gratefully acknowledge financial support from the National Natural Science Foundation of China (Grants 20703030, 20871092, and 20973125), the Key Project of Chinese Ministry of Education (Grant 209003), the Program for New Century Excellent Talents in University (Grant NCET-08-0914), and the Natural Science Foundation of Tianjin (Grants 10JCZDJC21600 and 10JCYBJC04800).

Supporting Information Available: TGA curves, PXRD patterns, additional figures and tables, and an X-ray crystallographic file in CIF format for **1** and **2**. This material is available free of charge via the Internet at http://pubs.acs.org. Crystallographic data for the structural analysis have also been deposited with the Cambridge Crystallographic Data Centre as CCDC 775710 and 742988 for **1** and **2**, respectively. These data can be obtained, upon request, from the Director, Cambridge Crystallographic Data Centre, 12 Union Road, Cambridge CB2 1EZ, U.K.

(56) Sain, S.; Maji, T. K.; Mostafa, G.; Lu, T.-H.; Rabis, J.; Tercero, X.; Chaudhuri, N. R. *Polyhedron* **2003**, *22*, 625.